Dephasing effects in a simple magnetic-breakdown linked-orbit network

Erik C. Sowa and L. M. Falicov
Department of Physics, University of California, Berkeley, California 94720
(Received 11 March 1985)

The magnetoresistivity of a magnetic-breakdown linked-orbit network with one-dimensional topology is calculated for the case of a stochastic distribution of defects in the network. We consider the case of a perfectly periodic network, as well as bimodal and rectangular distributions of defects. The results show an extremely pathological dependence on the defect distribution which is characteristic of the one-dimensional topology.

I. INTRODUCTION

The aim of this research is to understand, by means of model calculations, the effects of dephasing on the transport properties of electrons in a system where magnetic breakdown is present. The concept of magnetic breakdown (MB) in solids, first introduced over twenty years ago, is now an important piece of our understanding of the dynamics of band electrons in an applied magnetic field. The significance of the MB effect derives from its ability to alter drastically the topology of electron orbits as a function of magnetic field strength and orientation, and to form a system of orbits coupled probabilistically by a tunneling mechanism. First proposed by Cohen and Falicov[1] to explain the "giant orbit" observed in de Haas–van Alphen experiments in magnesium, MB is important in many experiments which are sensitive to the details of Fermi surface geometry. The way in which MB manifests itself in a given sample depends on the degree of coherence of the electronic wave functions in the applied fields; it is quite sensitive to the size and shape of the orbit network. In particular, if the purity of the sample is sufficient, quantum oscillations in the magnetoresistance (a giant Shubnikov–de Haas effect) may be observed, with phases of the oscillations proportional to the magnetic flux enclosed by the extremal closed orbits of the network.

Previous calculations of the magnetoresistance in MB-linked networks employed the Boltzmann equation and assumed perfect periodicity; they have yielded good agreement with experiment. However, even in relatively pure samples the periodicity may be broken by the presence of dislocations. They produce small changes in the areas of some closed orbits, which must result in some loss of coherence. The sensitivity of the magnetoresistance to these changes suggests using it to probe the distribution of the dislocations and study the way in which they affect the coherence of the electronic wave functions.

The basic physics of MB may be understood by considering Stark and Falicov's simple model[2] of a metal in which the Fermi "sphere" intersects only one Brillouin zone (BZ) boundary. Figure 1 shows a slab of the resulting Fermi surface in the repeated zone scheme, when a magnetic field perpendicular to the slab is applied. The electronic orbits are defined by the intersection of surfaces of constant energy with planes of constant wave vector parallel to the field. At low enough temperatures, only electrons at the Fermi energy are relevant. One therefore observes two types of orbits: the open orbits of the first BZ, and the lens orbits of the second BZ. When the electron wave packet comes to the intersection of the orbits, it experiences Bragg diffraction along the original orbit or tunnels across the gap into the next BZ. This latter effect, MB, results in a linked network of orbits. Though a full quantum-mechanical solution of the band structure in the presence of this effect is prohibitively complicated, one may describe such a system by means of Pippard's approach[3] of treating the orbits as a network with switching junctions wherever MB can occur. (This description is possible because in a metal one is typically in the semiclassical regime where the electronic wave functions are confined to a "racetrack" with a width that is negligible in comparison with its radius.) When MB is complete, one sees only a free-electron-like circle, which is a combination of portions of the open and lens orbits in a different sequence. Since the galvanomagnetic properties caused by open and closed orbits are very different, the topological effect of MB on the network has easily observable consequences, and the behavior in the intermediate regime of partially broken down junctions can be quite rich in structure.

Even within this switching-junction picture there are several levels of approximation. The most important consideration is whether or not the electrons maintain their quantum-mechanical phase coherence. The presence of

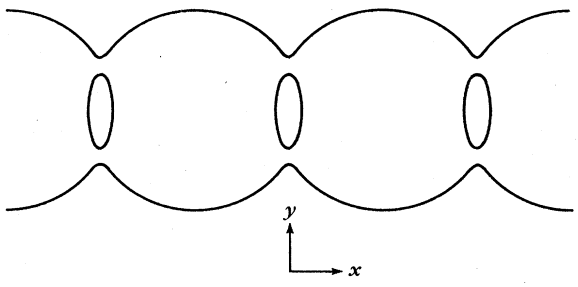

FIG. 1. Fermi surface of Stark and Falicov's model in the repeated zone scheme.

phase coherence gives rise to interference effects. For specific values of the magnetic field, destructive interference may result in zero probability of the electrons emerging from a junction onto the open-orbit path. These field values are not necessarily very large. When coherence is important, we may assign probability amplitudes to the branches of a switching junction as shown in Fig. 2. (For a justification of the basic MB formulas, see the review article by Stark and Falicov.[2]) In the absence of scattering, the amplitude of the wave function along any racetrack segment stays constant, while the phase changes according to the usual line integral of the vector potential.[3] At a junction, the wave function splits according to the probability amplitudes of Fig. 2. By adding up the amplitudes of all possible paths, one may follow the evolution of a wave packet on the network.

Large-angle scattering effects in the conductivity are well known,[4] and are accounted for by a relaxation time τ in the Boltzmann equation. On the other hand, small-angle scattering results in a wave packet staying on the racetrack but suffering a (random) change in phase, with the consequent loss of coherence. We consider the case where the lens orbit is so small that one may neglect scattering there, but the semicircular arms are long enough so that phase coherence is completely destroyed in the transit from one end of an arm to the other. The network [see Fig. 3(a)] reduces to "touching" circles on which only the amplitude is important, connected by nodes with transmission coefficient T and reflection coefficient $S\equiv 1-T$. These coefficients are calculated by injecting a wave packet of unit amplitude into the node [see Fig. 3(b)], adding up the infinite series of amplitudes obtained by letting the packet traverse many times the infinitesimal lens orbit until all of the probability has leaked out into one of the two available channels, and then taking the absolute square of the amplitudes thereby obtained. Clearly, for $T=1$ all trajectories correspond to open orbits, while for $T=0$ only the free-electron-like circles are observed. Since the phase change of the electron packet for a full lens orbit is just the magnetic flux through the lens, one expects the phase

$$\theta\equiv(A_R)H/(\hbar c/e)+\text{const}$$
$$=(A_k)(\hbar c/eH)+\text{const}$$

where A_R is the real-space area of the lens and A_k the k-space area, to be important. Indeed, one obtains the coefficients

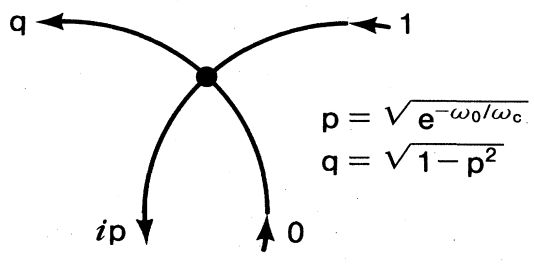

FIG. 2. Magnetic breakdown switching junction: probability amplitudes and phases.

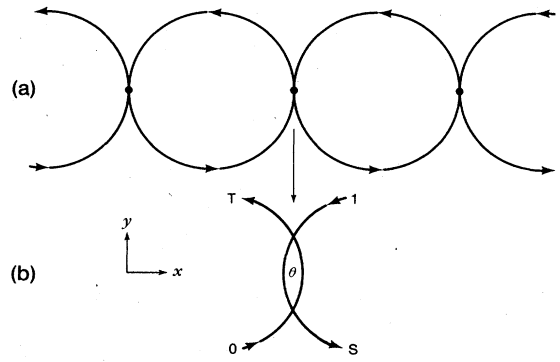

FIG. 3. (a) Model orbit network in k space. (b) Node connecting cells on the network.

$$T=\frac{2q^2(1-\cos\theta)}{1+q^4-2q^2\cos\theta}\quad\text{and}\quad S=\frac{p^4}{1+q^4-2q^2\cos\theta}$$

for Stark and Falicov's model, where p and q are defined in Fig. 3(b). Since the k-space area of the lens is a constant, T oscillates with the Shubnikov–de Haas period of the lens orbit between zero and $4q^2/(1+q^2)^2$, whereas S oscillates between one and $p^4/(1+q^2)^2$. As a consequence, transmission through the node may be periodically blocked ($T=0$), even at small field strengths.

In the next section, we use T and S to calculate the galvanomagnetic tensors for the network of Fig. 3(a). We allow for dislocations by assuming a stochastic distribution for the lens-orbit areas and taking ensemble averages of the observables over the probability distribution of these orbits. First we discuss the general formulation of the problem, then the low-field limit, then the infinite relaxation time limit, and finally our method of interpolating between these extremes. In Sec. III we show results for the cases of rectangular and bimodal distributions of lens areas, and we present our conclusions in the final section.

II. CALCULATION OF THE GALVANOMAGNETIC TENSORS

A. Formulation

The solution of the Boltzmann equation, in the uniform relaxation-time approximation by means of Chamber's effective path-integral method,[5] yields for the conductivity of the slab:

$$\overleftrightarrow{\sigma}=\frac{e^2}{(2\pi)^2}\sum_{\text{spin }\sigma}\int d^2k\,\mathbf{v}_{n\sigma}(k)\left[\frac{-df_0}{d\epsilon}\right]\mathbf{\Lambda}_{nk\sigma}\,,$$

where the effective path $\mathbf{\Lambda}_k$ is given by

$$\mathbf{\Lambda}_k\equiv\int_{-\infty}^{t_0(k)}dt\,\mathbf{v}_k(t)\exp\left[\frac{t-t_0}{\tau}\right]. \tag{1}$$

In (1), $\mathbf{v}_k(t)$ is the time-dependent group velocity of the wave packet, which satisfies the equations

$$\hbar\dot{\mathbf{k}}'=(e/c)[\mathbf{v}_{k'}(t)\times\mathbf{H}]\,,$$
$$\mathbf{v}_{k'}(t)=\hbar^{-1}(\partial\epsilon/\partial\mathbf{k}')\,,$$

such that the packet is at $k'=k$ at the time $t=t_0(k)$. Since the arms of the network are free-electron-like, their contribution to $\mathbf{\Lambda}_k$ is simple to evaluate. The effect of the nodes can be taken care of by matrix methods[2] whenever the coefficients at each node are the same throughout the network; however, we are explicitly interested in the case for which dislocations prevent this uniformity condition from being satisfied. Figure 4 shows the real-space orbit corresponding to the k-space network of Fig. 3(a). With this notation the effective path integral along the arms α and β of any given cell of the network becomes

$$\mathbf{\Lambda}(t,\alpha)=\mathbf{\Lambda}_A\exp(-t/\tau)+\int_0^t dt'\mathbf{v}(t',\alpha)\exp[(t'-t)/\tau]$$

and

$$\mathbf{\Lambda}(t,\beta)=\mathbf{\Lambda}_B\exp(-t/\tau)+\int_0^t dt'\mathbf{v}(t',\beta)\exp[(t'-t)/\tau]\ ,$$

where $\mathbf{\Lambda}_A$ and $\mathbf{\Lambda}_B$ are effective paths evaluated at the time ($t=0$) at which the electron wave packet emerges from a node onto the α and β arms, respectively. Thus if

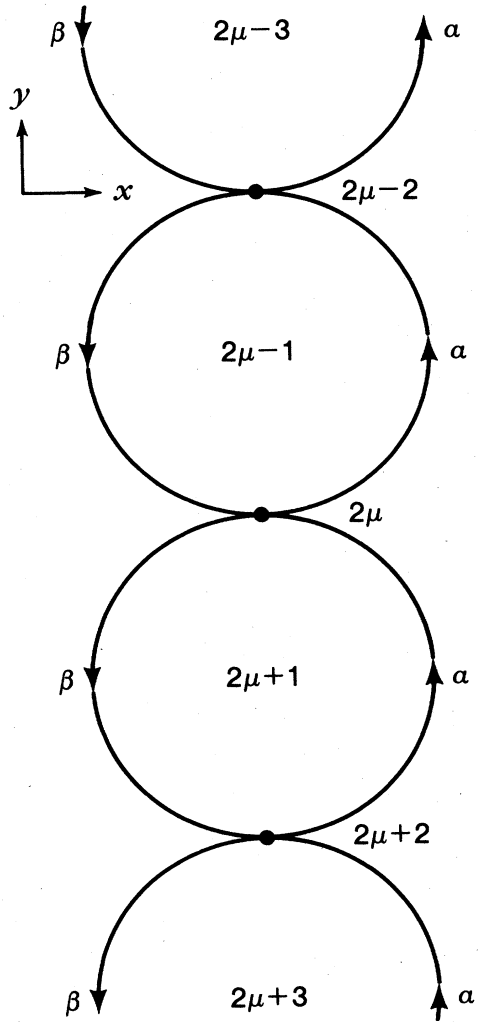

FIG. 4. Model orbit network in real space. We label nodes by even numbers $c=2\mu$ $(0,\pm2,\pm4,\ldots)$ and circular cells by odd numbers $d=2\mu+1$ $(\pm1,\pm3,\ldots)$.

$t_0=(\pi/\omega_c)$ is the travel time on one of the semicircular arms, and

$$\mathbf{L}_\alpha\equiv\int_0^{t_0}dt'\mathbf{v}(t',\alpha)\exp[(t'-t_0)/\tau]\ ,$$

$$\mathbf{L}_B\equiv\int_0^{t_0}dt'\mathbf{v}(t',\beta)\exp[(t'-t_0)/\tau]\ ,$$

then the effective path is given by the coupled equations[6]

$$\begin{aligned}\mathbf{\Lambda}_A(2\mu-1)&=T(2\mu)[\exp(-t_0/\tau)\mathbf{\Lambda}_A(2\mu+1)+\mathbf{L}_\alpha]\\&\quad+S(2\mu)[\exp(-t_0/\tau)\mathbf{\Lambda}_B(2\mu-1)+\mathbf{L}_\beta]\ ,\\\mathbf{\Lambda}_B(2\mu+1)&=T(2\mu)[\exp(-t_0/\tau)\mathbf{\Lambda}_B(2\mu-1)+\mathbf{L}_\beta]\\&\quad+S(2\mu)[\exp(-t_0/\tau)\mathbf{\Lambda}_A(2\mu+1)+\mathbf{L}_\alpha]\ .\end{aligned}\tag{2}$$

One may easily show that

$$\begin{aligned}\mathbf{L}_\alpha=-\mathbf{L}_\beta&=v_F\tau(1+\omega_c^2\tau^2)^{-1}\\&\quad\times[1+\exp(-t_0/\tau)](-\hat{\mathbf{x}}+\omega_c\tau\hat{\mathbf{y}})\ ,\end{aligned}$$

so in principle we have the algorithm necessary to calculate the effective path. To calculate the conductivity, which is proportional to $\mathbf{\Lambda}_k$, we must obtain the ensemble average of $\mathbf{\Lambda}$ over all possible orbits and orbit segments. In practice, we have not been able to solve exactly for this ensemble average of the effective path, but we have an approximation for the limit $\omega_c\tau\ll1$ and and exact solution for $\omega_c\tau\to\infty$. In what follows, we develop each of these in turn, and then discuss an interpolation scheme that connects them in the intermediate regime.

B. Low-field limit

When the area of the lens-shaped portion of the Fermi surface obeys a probability distribution, the matrix method[2] of solution mentioned earlier breaks down. Instead, one must follow a wave packet through the network by iterating Eq. (2), with each iteration following the packet for another unit of time t_0 and bringing in one more power of the coefficients $T(c)$ and $S(c)$. In order to perform correctly the ensemble average, it is convenient to find a recursion relation for $\mathbf{\Lambda}_A(d)$ and $\mathbf{\Lambda}_B(d)$, where d labels a cell on the network as in Fig. 4. If n is used to index the number of nodes that a particular contribution to the wave packet has encountered since being scattered onto the network, and a sum over all paths is performed, one obtains

$$\begin{aligned}\mathbf{\Lambda}_A(d)&=\left[\sum_{n=0}^{\infty}\lambda_A(n,d)\exp(-nt_0/\tau)\right]\mathbf{L}_\alpha\ ,\\\mathbf{\Lambda}_B(d)&=\left[\sum_{n=0}^{\infty}\lambda_B(n,d)\exp(-nt_0/\tau)\right]\mathbf{L}_\alpha\ ,\end{aligned}\tag{3}$$

with

$$\begin{aligned}\lambda_A(n,2\mu-1)&\equiv T(2\mu)\lambda_A(n-1,2\mu+1)\\&\quad+S(2\mu)\lambda_B(n-1,2\mu-1)\ ,\\\lambda_B(n,2\mu+1)&\equiv T(2\mu)\lambda_B(n-1,2\mu-1)\\&\quad+S(2\mu)\lambda_A(n-1,2\mu+1)\ ,\end{aligned}\tag{4}$$

and the initial conditions for (4)

$$\lambda_A(0,2\mu-1)=[T(2\mu)-S(2\mu)] \text{ and } \lambda_B(0,2\mu+1)=-[T(2\mu)-S(2\mu)] .$$

This yields a partial contribution to σ of the form

$$\Delta\vec{\sigma}=\frac{\sigma_0\omega_c\tau}{\pi[1+(\omega_c\tau)^2]}[1+\exp(-t_0/\tau)]^2\sum_n \exp(-nt_0/\tau)[\lambda_A(n,2\mu-1)-\lambda_B(n,2\mu+1)]\begin{bmatrix}-1 & \omega_c\tau\\ -\omega_c\tau & (\omega_c\tau)^2\end{bmatrix}, \tag{5}$$

where σ_0 is the $H=0$ conductivity of the slab. Thus if we know $O(n,\mu)\equiv[\lambda_A(n,2\mu-1)-\lambda_B(n,2\mu+1)]$, we have $\vec{\sigma}$ and therefore also the resistivity $\vec{\rho}$. Defining

$$E(n,\mu)\equiv[\lambda_A(n,2\mu-1)+\lambda_B(n,2\mu+1)] ,$$

the recursion relations (4) may be rewritten as

$$E(n,\mu)=(\tfrac{1}{2})[E(n-1,\mu+1)+E(n-1,\mu-1)+O(n-1,\mu+1)-O(n-1,\mu-1)] ,$$

$$O(n,\mu)=(\tfrac{1}{2})[E(n-1,\mu+1)-E(n-1,\mu-1)+O(n-1,\mu+1)+O(n-1,\mu-1)] ,$$

with the initial conditions

$$E(0,\mu)=0 \text{ and } O(0,\mu)=2[T(2\mu)-S(2\mu)] .$$

Of course, the number of terms in $O(n,c)$ grows geometrically with n; however, in the limit $\omega_c\tau\ll 1$ one may cut off the iteration after a few terms due to the damping factor $\exp(-t_0/\tau)$ in (3). Then one must correctly average the powers of $[T(2\mu)-S(2\mu)]$ over the distribution of the lens areas.[7] As an example, the term for $n=2$ is

$$\begin{aligned}O(2,\mu)=(\tfrac{1}{2})[T(2\mu)-S(2\mu)]([T(2\mu)-S(2\mu)]\{[T(2\mu+2)-S(2\mu+2)]+[T(2\mu-2)-S(2\mu-2)]-2\}\\ +[T(2\mu+4)-S(2\mu+4)]\{1+[T(2\mu+2)-S(2\mu+2)]\}\\ +[T(2\mu-4)-S(2\mu-4)]\{1+[T(2\mu-2)-S(2\mu-2)]\}) ,\end{aligned}$$

which averages to

$$\langle O(2)\rangle=\langle T-S\rangle^3+\langle T-S\rangle^2+\langle T-S\rangle\langle(T-S)^2\rangle-\langle(T-S)^2\rangle .$$

This procedure in principle may be laboriously extended to ever higher orders; as the damping factor $\exp(-t_0/\tau)$ approaches 1 for $\omega_c\tau\gg 1$, higher orders of $\langle O(n)\rangle$ are necessary in Eq. (3) and the work required becomes prohibitive. Because we are interested in the ensemble-averaged effective path for all field values, it is necessary to consider the opposite limit $\omega_c\tau\to\infty$.

C. Infinite relaxation time limit

When large-angle scattering may be ignored, the relaxation time becomes infinite and the damping factor becomes one. Equation (2) reduces to

$$\Lambda_A(2\mu-1)=T(2\mu)\Lambda_A(2\mu+1)+S(2\mu)\Lambda_B(2\mu-1) ,$$

$$\Lambda_B(2\mu+1)=T(2\mu)\Lambda_B(2\mu-1)+S(2\mu)\Lambda_A(2\mu+1) .$$

This simpler form may be solved by use of transfer-matrix techniques. With $r(c)\equiv S(c)/T(c)$ and a little rearrangement we find the matrix equation

$$\begin{bmatrix}\Lambda_B(2\mu+1)\\ \Lambda_A(2\mu+1)\end{bmatrix}=\begin{bmatrix}1-r(2\mu) & r(2\mu)\\ -r(2\mu) & 1+r(2\mu)\end{bmatrix}\begin{bmatrix}\Lambda_B(2\mu-1)\\ \Lambda_A(2\mu-1)\end{bmatrix} .$$

This is easily iterated to yield

$$\begin{bmatrix}\Lambda_B(2\mu+2N+1)\\ \Lambda_A(2\mu+2N+1)\end{bmatrix}=\begin{bmatrix}1-R_N & R_N\\ -R_N & 1+R_N\end{bmatrix}\begin{bmatrix}\Lambda_B(2\mu-1)\\ \Lambda_A(2\mu-1)\end{bmatrix},$$

where

$$R_N\equiv\sum_{n=0}^{N} r(2\mu+2n) .$$

Thus in this limit we need the average of $r\equiv S/T$ over the probability distribution. A straightforward calculation now yields for the sum in the right-hand side of Eq. (5)

$$\sum_n \exp(-nt_0/\tau)\langle O(n)\rangle\to(1/\langle S/T\rangle-1)\equiv\Sigma . \tag{6}$$

This limit has some interesting physical consequences to be discussed later.

D. Interpolation scheme

There are two contributions to $\vec{\sigma}$. The first comes strictly from scattering on the semicircular arms of the network, and is known exactly for all values of $\omega_c\tau$. The second is the $\Delta\vec{\sigma}$ of Eq. (5). If this could be evaluated for all $\omega_c\tau$, the problem would be solved; however, we know it only for $\omega_c\tau\ll 1$ and $\omega_c\tau\to\infty$. This suggests an interpolation scheme to connect the solutions in the intermediate regime. The important quantity is Φ, the ensemble-averaged summation over $O(n,\mu)$:

$$\Phi(\omega_c\tau)=\sum_{n=0}^{\infty}\langle O(n)\rangle\exp(-nt_0/\tau) , \tag{7}$$

which has the infinite relaxation time limit $\Phi(\infty)=\Sigma$,

given in Eq. (6). Cutting off the series at the Nth term yields a correct low-field limit, but the neglected terms are important for $\omega_c\tau \gg 1$. A reasonable interpolation scheme, exact in both limits, suggests itself:

$$\langle \Phi_N \rangle = \sum_{n=0}^{N} \langle O(n) \rangle \exp(-nt_0/\tau) + \exp[-(N+1)t_0/\tau] \left[\Sigma - \sum_{n=0}^{N} \langle O(n) \rangle \right] . \quad (8)$$

In words, we evaluate exactly the series up to $n=N$ [the first term in (8)]. To this we add the $n>N$ end of the series, evaluated for $\omega_c\tau \to \infty$ and multiplied by the power of the damping factor appropriate for $n=N+1$ [the second term in (8)]. This procedure overestimates the contributions from the large-n terms. However, in the low-field case this overestimation is rendered unimportant by the prefactor $\exp[-(N+1)t_0/\tau]$, whereas in the opposite limit the prefactor is very nearly one in any case, making the overestimate insignificant.

Because of the way we perform the calculation by successive iterations, our interpolation scheme gives an alternating sequence for $\langle \Phi_N \rangle$ for any given relaxation time as the magnetic field goes to infinity. This alternation is not important since it only happens at extremely high fields, and the average of successive even and odd approximations gives the correct infinite limit. We have therefore chosen to average $\langle \Phi_{2N-2} \rangle$ and $\langle \Phi_{2N-1} \rangle$; it generates what we ultimately call the Nth approximation to the effective path. Keeping this in mind, from this point on $\langle \Phi \rangle$ will be used to denote this average, with N understood to mean the average of the $(2N-2)$ and $(2N-1)$ approximations of Eq. (8).

E. The galvanomagnetic tensors

By defining

$$Z_N \equiv \{2+[1+\exp(-t_0/\tau)]\langle \Phi \rangle\}(\omega_c\tau)^2[1+\exp(-t_0/\tau)] \times \{\pi[1+(\omega_c\tau)^2]\}^{-1} ,$$

the complete expression for the conductivity tensor may be written

$$\vec{\sigma} = \frac{\sigma_0}{1+(\omega_c\tau)^2} \begin{bmatrix} 1-Z_N/\omega_c\tau & -(\omega_c\tau - Z_N) \\ (\omega_c\tau - Z_N) & 1+\omega_c\tau Z_N \end{bmatrix} .$$

It is easy to invert the tensor to obtain the diagonal component of the resistivity along the network:[8]

$$\rho_{11} = (\omega_c\tau/\sigma_0)\frac{1+\omega_c\tau Z_N}{\omega_c\tau - Z_N} = \frac{m\omega_c}{ne^2}\frac{(1+\omega_c\tau Z_N)}{(\omega_c\tau - Z_N)} . \quad (9)$$

In Sec. III we present our results for ρ_{11} for several interesting cases.

F. Accuracy of the interpolation scheme

We compare our result for a perfect network (delta-function distribution for the lens-orbit areas) with the result[5] by the standard method, exact for arbitrary relaxation time, to test the accuracy of the interpolation scheme for intermediate values of $\omega_c\tau$. Figure 5(c) is the exact result for this network when $\omega_c\tau=1$, whereas in Fig. 5(b) we have shown our $N=3$ approximation. Comparison clearly shows that the interpolation scheme is indeed excellent.

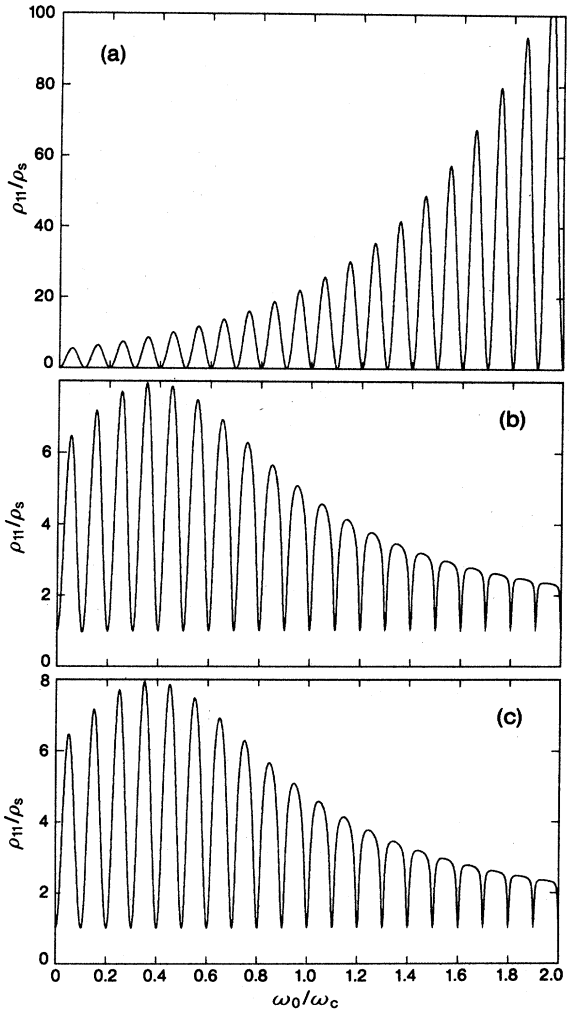

FIG. 5. (a) Exact result for ρ_{11} with 1.0 probability for θ_2 and $\omega_0\tau \to \infty$. (b) The $N=3$ approximation for ρ_{11} with 1.0 probability for θ_2 and $\omega_0\tau=1$. (c) Exact result for ρ_{11} with 1.0 probability for θ_2 and $\omega_0\tau=1$.

III. RESULTS

In our model, the convenient unit to measure magnetic fields is the magnetic breakdown frequency $\omega_0 \equiv eH_0/mc$, and the convenient resistivity unit is $\rho_s \equiv (\omega_0\tau/\sigma_0) = (m\omega_0/ne^2)$. Our results are therefore plots of ρ_{11}/ρ_s vs (ω_0/ω_c) for various distributions. Relaxation times are in units of $1/\omega_0$.

The k-space area of the lens orbit is given probabilistically. In each of our cases two phases, θ_1 and θ_2, are im-

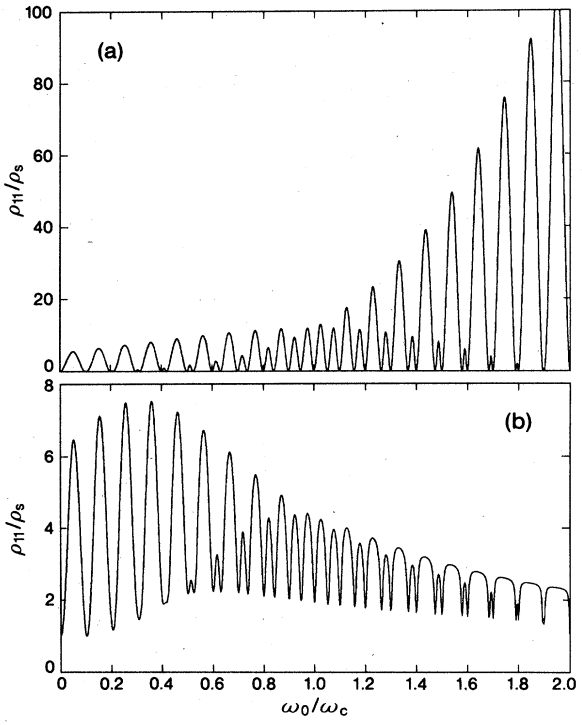

FIG. 6. (a) Exact result for ρ_{11} with 0.5 probability for θ_1, 0.5 probability for θ_2, and $\omega_0\tau\to\infty$. (b) The $N=3$ approximation for ρ_{11} with 0.5 probability for θ_1, 0.5 probability for θ_2, and $\omega_0\tau=1$.

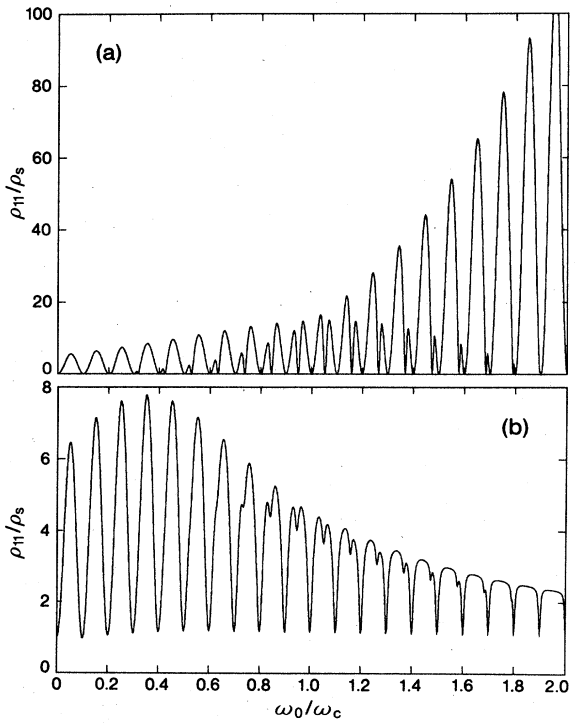

FIG. 7. (a) Exact result for ρ_{11} with 0.1 probability for θ_1, 0.9 probability for θ_2, and $\omega_0\tau\to\infty$. (b) The $N=3$ approximation for ρ_{11} with 0.1 probability for θ_1, 0.9 probability for θ_2, and $\omega_0\tau=1$.

portant. We choose the corresponding areas of the lens such that at $\omega_c=\omega_0$, the two relevant phases are $\theta_1=2\pi(9.5)$ and $\theta_2=2\pi(10.0)$. The results for finite relaxation time are all calculated to the $N=3$ approximation, except when explicitly indicated otherwise; the infinite relaxation time results are all derived by the transfer-matrix method of Sec. II C.

In Fig. 5 we have shown the resistivity for the case of pure θ_2. The first plot is for infinite relaxation time. Note that when $\theta=2n\pi$, the opaque nodes drive ρ_{11} to zero. The rise of the envelope is caused by the increase of transmission as the field becomes weaker and MB is reduced. In the second plot the relaxation time is $\omega_0\tau=1$. The effective path decreases as the field gets weaker, and the upper envelope of ρ_{11} passes through a maximum. The periodic minima have risen to positive values, and become narrower as the field decreases.

The same relaxation times for a bimodal distribution (0.5 probability for θ_1 and 0.5 probability for θ_2 in one case, and 0.1 for θ_1 and 0.9 for θ_2 in the other) yield the results shown in Figs. 6 and 7, respectively. The general features are the same as in Fig. 5. A decrease in the relaxation time tends to smear out the minority frequency, but the minima due to either frequency persist.

The most interesting case is the rectangular distribution that gives equal probability to any phase between θ_1 and θ_2, and is zero otherwise. Figure 8 shows this case for infinite relaxation time. The most striking features are the bands of zeros that get wider as the field decreases, and the turnover of the envelope as if some scattering were taking place. Of course, the minima correspond to the situation $\theta_1\leq 2n\pi\leq\theta_2$. In this case the field value is such that there is a finite probability that somewhere in the network one of the nodes has turned opaque. Because in the $\omega_c\tau\to\infty$ limit the electrons never scatter off the network, when even one junction is opaque, the network cannot carry current. This feature is peculiar to the one-dimensional topology of the model, and may be compared to a water pipe with many valves in series. When just one valve is shut, the flow of water ceases no matter how the

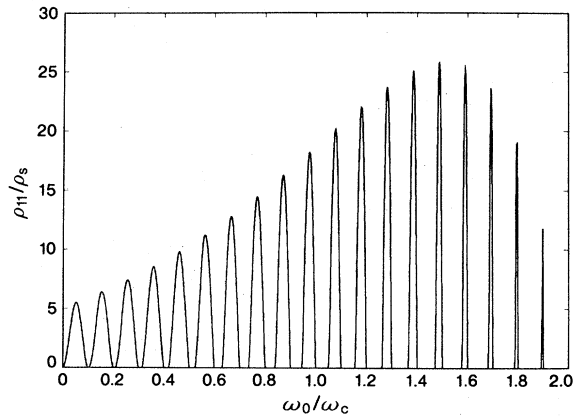

FIG. 8. Exact result for ρ_{11} with rectangular distribution and $\omega_0\tau\to\infty$.

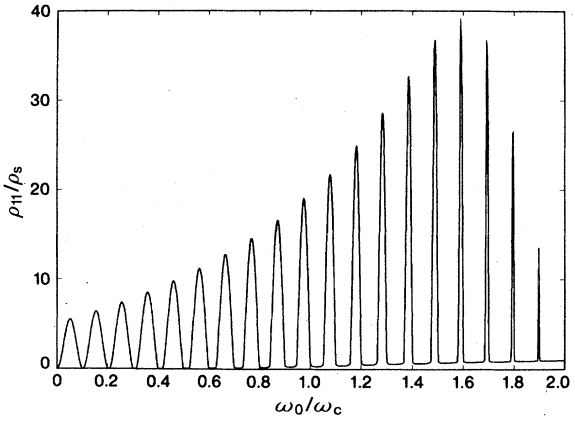

FIG. 9. The $N=3$ approximation for ρ_{11} with rectangular distribution and $\omega_0\tau=100$.

other valves are set. The cause of the turnover of the envelope can be thought of as due to an effective "dephasing" scattering.

A finite relaxation time corresponds, in our water pipe analog, to drilling a few holes in the pipe between the valves. Even if the values are shut, water pressure can generate a flow since water can leak out through the holes. A finite relaxation time should therefore round off the edges of the minima in the resistivity and raise them from zero to positive values. Figures 9—12, plots for the same rectangular distribution with $\omega_0\tau=100$, 10, 1, and 0.1, respectively, show this effect. (Figure 11 actually shows three plots with $\omega_0\tau=1$. These are the successive approximations $N=1$, 2, and 3, and are shown to demonstrate qualitatively that our interpolation scheme converges quickly.) As the field becomes weaker, the minima regions get wider, and the Shubnikov—de Haas oscillations damp down to a single line. Randomness ends up destroying the connectivity of the MB-linked network.

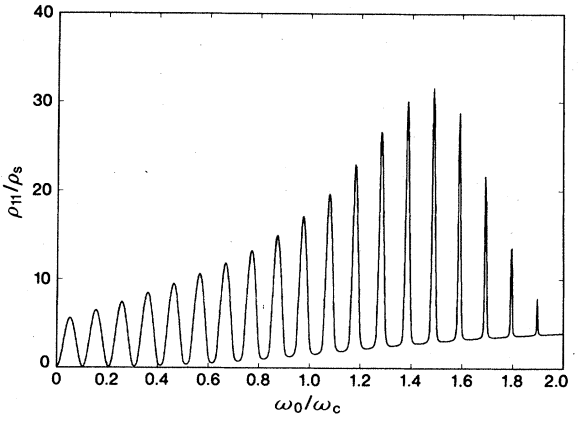

FIG. 10. The $N=3$ approximation for ρ_{11} with rectangular distribution and $\omega_0\tau=10$.

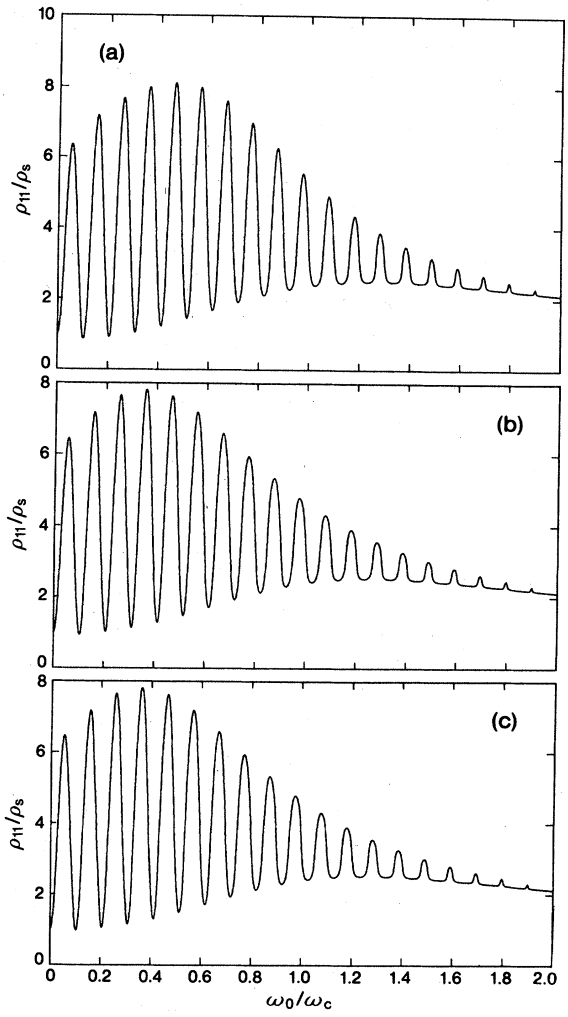

FIG. 11. (a) The $N=1$ approximation for ρ_{11} with rectangular distribution and $\omega_0\tau=1$. (b) The $N=2$ approximation for ρ_{11} with rectangular distribution and $\omega_0\tau=1$. (c) The $N=3$ approximation for ρ_{11} with rectangular distribution and $\omega_0\tau=1$.

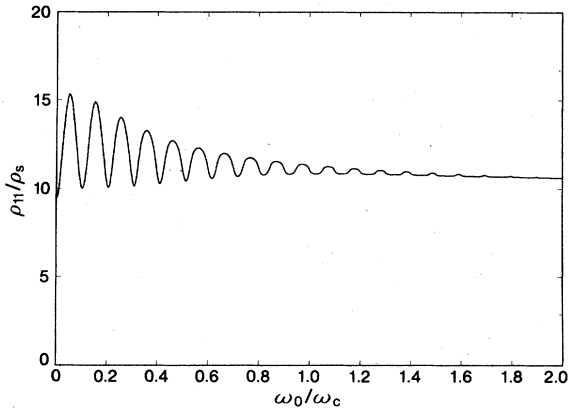

FIG. 12. The $N=3$ approximation for ρ_{11} with rectangular distribution and $\omega_0\tau=0.1$.

IV. CONCLUSIONS

Our model is just one example of phase-coherent galvanomagnetic effects in magnetic breakdown networks. There is a huge range of possibilities as the network topology and dynamics change.[9–12] In this section, we discuss the special features of our results and model which are particularly interesting.

Our results demonstrate the danger of assuming that a small quantity of dislocations necessarily has very little influence on the transport effective path. The dephasing effect in our model provides a mechanism by which the effective path decreases drastically, even in the case of very small changes in the distribution of k-space areas. The main reason for this is the overwhelming importance of the particular phase that causes a node to become opaque ($T=0$), which is a feature characteristic of the one-dimensional topology of the network. A small quantity of nodes with this opaque phase is much more significant to transport on the entire network than the same small quantity with any other phase. This is especially true at smaller values of $\omega_c\tau$. In Fig. 7(b) ($\omega_0\tau=1$), just 1% concentration of the minority phase has an easily observable effect on ρ_{11}, but only when the field strength is such that this minority phase produces an opaque junction. The effect is even more dramatic when there is a continuous distribution for the areas. The resistivity derived from the rectangular distribution (Figs. 8–12) is qualitatively and quantitatively very different from that derived from a single well-defined area (Fig. 5), because the finite width of the distribution gives rise to finite bands of field values for which some node in the network becomes opaque.

The highly nonlinear dependence of the effective path on the distribution of k-space areas contrasts sharply with the usual effects of impurities (i.e., relaxation rates). It suggests that even small quantities of dislocations (or other area-changing imperfections) might be detectable in the right kind of crystal. The one-dimensional topology of the network is responsible for the pathological behavior. Systems with one-dimensional topology exist. Highly pure magnesium for fields in the basal plane has a one-dimensional coupled network of orbits. Its nodes are more complex than the simple lens orbit of our model, and quantum coherence on the larger orbit segments can cause further complications which we have not considered.[13] Another type of system, typified by graphite intercalation compounds such as stage 1 AsF_5 graphite, holds more promise for finding the dephasing effect. These crystals are two-dimensional in character and may have orbit networks very similar to that of our model.[14] Such a topology would occur if the usual periodicity of the crystal in the graphite plane were doubled along one crystal axis but not along the other, causing the (usually hexagonal) Brillouin zone to fold over into a rectangle of half the area. If the carrier concentration is such that the fold in the BZ touches the edge of the Fermi surface, the result is similar to the BZ of Fig. 1. It would be very interesting to see the results of a magnetoresistance experiment on a system like AsF_5 graphite with purity such that the nodes are fully coherent and the arms are, in essence, semiclassical.

ACKNOWLEDGMENT

This work was supported in part by the National Science Foundation through Grant No. DMR81-06494.

[1]M. H. Cohen and L. M. Falicov, Phys. Rev. Lett. **7**, 231 (1961).
[2]R. W. Stark and L. M. Falicov, in *Progress in Low Temperature Physics*, edited by C. J. Gorter (North-Holland, Amsterdam, 1967), Vol. 5, p. 235.
[3]A. B. Pippard, Proc. R. Soc. London, Ser. A **270**, 1 (1962).
[4]J. M. Ziman, *Principles of the Theory of Solids*, 2nd ed. (Cambridge University, Cambridge, England, 1972), Chap. 7.
[5]L. M. Falicov, *Electrons in Crystalline Solids* (IAEA, Vienna, 1973), pp. 256–259.
[6]We label nodes by even numbers $c=2\mu$ $(0,\pm2,\pm4,\ldots)$ and circular cells by odd numbers $d=2\mu+1$ $(\pm1,\pm3,\ldots)$.
[7]We assume a Markovian process where the stochastic distribution of probabilities at each node is independent of all other nodes.
[8]This is the only interesting component of $\vec{\rho}$.
[9]L. M. Falicov and P. R. Sievert, Phys. Rev. **138**, A66 (1965).
[10]L. M. Falicov, A. B. Pippard, and P. R. Sievert, Phys. Rev. **131**, 498 (1966).
[11]C. E. T. Gonçalves da Silva and L. M. Falicov, Phys. Rev. B **8**, 527 (1973).
[12]P. Thalmeier and L. M. Falicov, Phys. Rev. B **23**, 2586 (1981).
[13]N. B. Sandesara and R. W. Stark, Phys. Rev. Lett. **53**, 1681 (1984).
[14]R. S. Markiewicz, C. Zahopoulos, D. Chipman, J. Mulliken, and J. E. Fischer, private communication.